Magneto-optic gradient effect in domain-wall images: At the crossroads of magneto-optics and micromagnetics

V. Kamberský
Institute of Physics, Academy of Sciences of the Czech Republic, Cukrovarnická 10, 162 53 Praha 6, Czech Republic

R. Schäfer
Leibniz Institute for Solid State and Materials Research, Helmholtzstrasse 20, 01069 Dresden, Germany

(Received 30 March 2011; published 15 July 2011)

An anomalous symmetry of magneto-optical images of ferromagnetic domain walls was reported by Schäfer and Hubert [Phys. Status Solidi A **118**, 271 (1990)] and interpreted in terms of light amplitudes proportional to the magnetization gradient. We present analytic and numerical calculations supporting such proportionality under additional conditions implied by classical rules of micromagnetics and address some objections presented by Banno [Phys. Rev. A **77**, 033818 (2008)] against such proportionality.

DOI: 10.1103/PhysRevA.84.013815 PACS number(s): 42.25.Gy, 42.25.Fx, 78.20.Ls, 78.20.Bh

I. INTRODUCTION

The magneto-optic (MO) images of magnetic domain boundaries reported in Ref. [1] attracted considerable attention due to the unexpected symmetry with respect to light polarization. The images appeared in a polarization microscope as bright and dark lines on the sample surface and the contrast was reversed on rotation of the polarizer by 90°, which is characteristic for linear birefringence; as in the Voigt effect [1], the domain magnetization was parallel to the sample surface. The observed patterns were of two types, with different sets of birefringence axes and different gradients of the magnetization direction vector **m**. When (i) only the **m** component parallel to the wall varied, the main axes were parallel and normal to the wall. But when (ii) the **m** component normal to the wall line varied across the wall, the main axes were at ±45° to the wall line i.e., the MO contrast was largest when the polarizer axis was parallel or normal to the wall line; this included cases with the surface domain **m** parallel to the **E** field of the incident light, although in such cases the MO interaction in the classical dielectric law

$$\mathbf{D} = \varepsilon(\mathbf{E} + iQ\mathbf{m} \times \mathbf{E}) \tag{1}$$

is expected to vanish. The authors [1] found that all features of the observed images were consistent with an extension of the dielectric law in Eq. (1), with additional components of **D** at the surface; these were described as

$$D_\eta^{(s)} = P\left(\frac{\partial m_\xi}{\partial \xi} - \frac{\partial m_\eta}{\partial \eta}\right) E_\xi \tag{2}$$

in the special coordinate system where ξ and η denote the axes of the polarizer and (crossed) analyzer and subsequently generalized [1,2]. The parameter P was found to be proportional to Q in Eq. (1) in a variety of materials [1]. The first term in Eq. (2), containing a product of mutually parallel components m_ξ and E_ξ, was particularly required for description of type (ii) patterns.

The full symmetry of the wall images [1] could not be explained from MO diffraction and the dielectric law [Eq. (1)] alone. In an early brief note [3] only the last term in Eq. (2) was derived from diffraction on **m** gradient components parallel to the sample surface. Intuitive discussions [4,5] of this particular effect pointed out the role of MO polarization normal to the sample surface (and corresponding surface charges) with a gradient and thus a depolarizing **E** field pointing across the domain wall.

The failure to explain the controversial first term in Eq. (2) and the contrast in type (ii) structures was pointed out by A. Hubert in seminal discussions. An improved analysis of type (ii) contrast [6] took into account also the polar Kerr effect caused by **m** components perpendicular to the sample surface in the subsurface region in type (ii) structures schematically shown in Fig. 1. Some role of subsurface polar Kerr effect was originally suspected [1], but its symmetry of circular rather than linear birefringence was reconciled with the experimental results only later [6], taking into account the correlation between the planar and polar **m** gradient implied by the micromagnetic conditions of magnetic flux closure in soft magnetic materials [7–9]. The full angular dependence of the wall contrast [1] was thus derived analytically [6,10] and discussed in the context of MO depth sensitivity [10,11] and of phenomenological MO tensors sensitive to the **m** gradient [1,2,12].

In the original version of Ref. [5] the gradient phenomenology [1] was stated to be physically unacceptable because of an apparent divergence of the magnetization gradient. Consequently, the previous work [1,10] was not reviewed correctly in several respects (see item 2 in Ref. [5]).

In this paper it is first shown in detail that the gradient phenomenology, Eq. (2), leads to the observed angular dependence [1] of the wall images and the objections [5] were not justified. An additional section reviews and augments the argument supporting the correctness of descriptions of the domain wall images [1] in terms of the magnetization gradient. It is stressed that the adequacy of linear gradient approximations and the symmetry of the effect are due, respectively, to the relatively large domain wall widths and to the tendency to magnetic flux closure (i.e. to the elementary micromagnetic rules formulated by Landau and Lifshits [7]).

II. EMPIRICAL EQUATIONS

To show that Eq. (2) leads to the observed angular symmetry of the intensity of the wall images (integrated across the wall

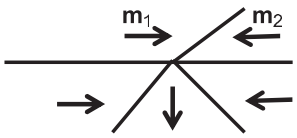

FIG. 1. Schematic V-line structure

width [1]), consider that **m** varies only along the wall normal, identified further with the y axis (Fig. 2). The gradient of any function $f(y)$ has components along the polarizer and analyzer axes ξ and η equal to

$$\frac{\partial f}{\partial \xi} = \frac{df}{dy}\cos\gamma \tag{3a}$$

$$\frac{\partial f}{\partial \eta} = \frac{df}{dy}\sin\gamma, \tag{3b}$$

where γ is the angle between the ξ and y axes. Using these relations for both m_ξ and m_η in Eq. (2) and integrating across the wall we get

$$\int D_\eta^{(s)} dy = -P(S_\xi \cos\gamma - S_\eta \sin\gamma)E_\xi \tag{4a}$$

where $\mathbf{S} = \mathbf{m_1} - \mathbf{m_2}$ is the difference of the unit vectors $\mathbf{m_{1,2}}$ in the two domains (Fig. 2). Its ξ and η components are equal to $|\mathbf{S}|\cos\alpha$ and $|\mathbf{S}|\sin\alpha$ where α is the angle between the ξ axis and **S**. Thus

$$\int D_\eta^{(s)} dy = -P|\mathbf{S}|\cos(\alpha+\gamma)E_\xi, \tag{4b}$$

which agrees with the equation for the integrated contrast in the original report [1], where $|\mathbf{S}|$ is written as $2\sin(\Omega/2)$ and Ω is the angle between $\mathbf{m}_1$ and $\mathbf{m}_2$ (Fig. 2). The compact angular factor in Eq. (4) may be written as $\cos(2\gamma+\delta)$, where δ is the angle between y and **S**, fixed in the magnetic structure, and the argument 2γ shows clearly the periodicity of linear birefringence. Since $|\mathbf{S}|\cos\delta = \mathbf{S_y}$ and $|\mathbf{S}|\sin\delta = \mathbf{S_x}$ are the components of **S** along the wall normal and the wall direction, respectively, the empirical Eq. (4b) may also be written as

$$\int D_\eta^{(s)} dy = P(S_x \sin 2\gamma - S_y \cos 2\gamma)E_\xi, \tag{4c}$$

which shows separately the effects connected with the two kinds of magnetization gradient, mentioned in the preceding section as type (i) and type (ii).

In the first version of Ref. [5], the factors $\cos\gamma$ and $\sin\gamma$ in the gradient transforms used instead of present Eq. (3) appeared as divisors instead of multipliers, which led to spurious divergence of the angular dependence and to unjustified critique of the gradient model [1] (see item 2 in Ref. [5] for corrections).

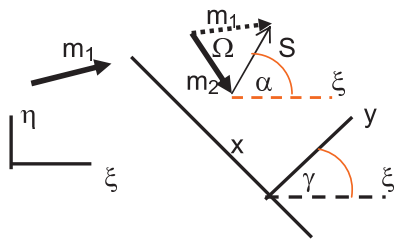

FIG. 2. (Color online) Angles and axes characterizing magnetization directions in the surface domains (after Ref. [1]).

III. MAGNETO-OPTIC DIFFRACTION

Standard perturbation theory [10], as applied earlier to diffraction on domain walls [13] and to scattering on spin waves [14], uses the MO polarization $\mathbf{P^{(m)}} = \mathbf{iQ}\varepsilon\mathbf{m} \times \mathbf{E^0}$ from Eq. (1) as the source of the first-order scattered $\mathbf{E^1}$, while $\mathbf{E^0}$ is the zero-order field corresponding to $Q = 0$. For normal incidence of light, in the coordinates shown in Fig. 2 (and $e^{-i\omega t}$ dependence), the scattered field amplitudes $E^1_{x,y}$ may be expanded as

$$E_r^1(y,z) = \int E_r'^1(q,z)e^{iqz}dq. \tag{5}$$

The relations between the amplitudes $E_r'^1$ and $E^0_{r'}$ depend on the $m'_{r'}(q,z)$ components of similar Fourier expansions of $m_{r'}(y,z)$ in the whole depth of light penetration, with complex retardation factors taking into account the path from 0 to z and back: $\phi(z) = e^{i(k+k')z}$ with the propagation constants $k = 2\pi n/\lambda$ for $E^0_r(z)$ and $k' = (k^2 - q^2)^{1/2}$ for $E^1_r(q,z)$, if n is the refraction index and λ the vacuum wavelength. The result for $E^1_r(q)$ at the $z = 0$ surface is a superposition of four terms

$$E_y'^1(q)^{(mx)} = -Qq\int m'_x(q,z)\phi(z)dz E^0_y t_y, \tag{6a}$$

$$E_y'^1(q)^{(my)} = Qq\int m'_y(q,z)\phi(z)dz E^0_x t_y, \tag{6b}$$

$$E_y'^1(q)^{(mz)} = -Qk'\int m'_z(q,z)\phi(z)dz E^0_x t_y, \tag{7a}$$

$$E_x'^1(q)^{(mz)} = Qk\int m'_z(q,z)\phi(z)dz E^0_y t_x. \tag{7b}$$

The superscripts (mr) denote the active **m** component. For thick samples, the integrals run from 0 to ∞ and the factors $t_{x,y}$ (listed in Appendix A) are close to $n/(n+1)$ for $|q/k|^2 \ll 1$. Equations (7a) and (7b) describe the Kerr effect due to polar magnetization, m_z. Equations (6a) and (6b) involve directly the Fourier components of the planar magnetization gradient across the wall, $iqm_{x,y}(q,z)$, which causes a corresponding gradient of the MO polarization current, $-i\omega P_z^{(m)}$ normal to the surface. Similar terms cause the well-known transverse and longitudinal Kerr effects at skew light incidence in the y-z plane [10], then $P_z^{(m)}$ varies along y due to variations of E^0_y and E^0_x, respectively.

Support for the empirical linear gradient approximation is discussed below with regard to two basic micromagnetic aspects: (i) the relatively large wall width and (ii) the tendency to magnetic flux closure.

A. Gradient approximation

In the classical Bloch wall [7] only the **m** components parallel to the wall vary and the images of the m_x gradient are described by Eq. (6a). In the classical wall model [7] $m_x(y)$ varies as $\tanh(y/w_0)$ and the transform $m'_x(q)$ is equal [13] to $w_0/2i\sinh(\pi q w_0/2)$ with an obvious exponential cutoff. The plot of the image field E^1_y generated at the surface is shown in Fig. 3 (for $n = 2.9 + 3.1i$ for iron, $\lambda = 633$ nm and a

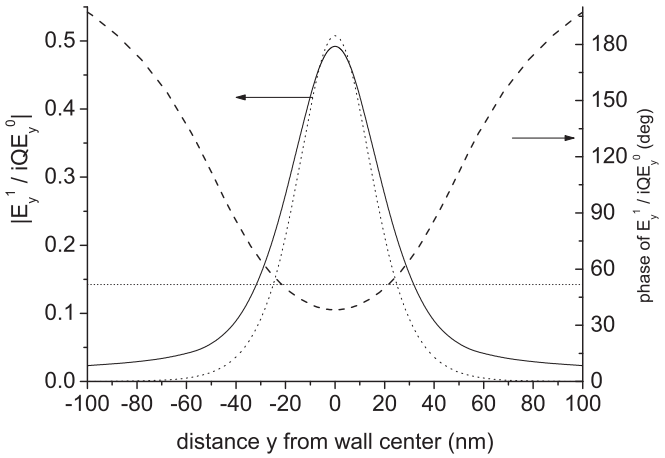

FIG. 3. Profile of the normalized MO amplitude $E^1(y)$: absolute value (solid line), phase (dashed line), and the gradient approximation (dotted lines) (phase is constant) generated at the surface by $m_x = \tanh(y/w_0)$ in the classical wall model [7,13].

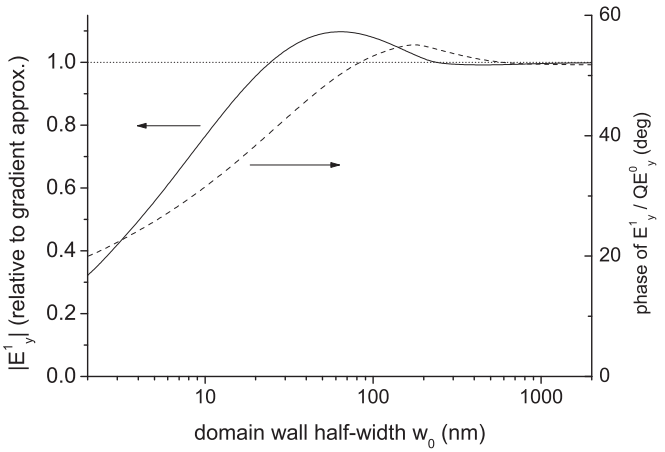

FIG. 4. Normalized MO amplitude $E^1(y)$ at wall center (y=0) vs wall half-width w_0: absolute value relative to the gradient approximation (solid line), phase (dashed line), gradient approximation (dotted line), model and parameters as in Fig. 3.

rather small value of $w_0 = 20$ nm). The solid line shows the normalized absolute value $|E_y^1/iQE_y^0|$. It is remarkably close to the corresponding plot of the gradient approximation (dotted line)

$$E_y^{1a}(y) = -B\frac{dm_x}{dy}E_y^0 \tag{8a}$$

$$B = \frac{Q\lambda}{4\pi(n+1)} \tag{8b}$$

Also the phase of the normalized image field (dashed line) in the central part of the image is close to the constant phase of the approximation in Eq. (8) (dotted line). The approximation in Eq. (8) follows from first-order expansions in components of the magnetization gradient [12]. Derivation from Eqs. (5) and (6a) assumes that $|q/k|^2 \ll 1$ in a substantial part of the $m_x(q)$ spectrum, so that $k' \simeq k$ and $t_y \simeq n/(n+1)$. Then $\int m_x(q)e^{iqz}dq$ in Eq. (5) gives $-i\partial m_x/\partial y$ and the remaining $\int \phi(z)dz$ in Eq. (6a), gives $i/2k = i\lambda/4\pi n$. Such approximation is adequate in relatively wide domain walls, with $|kw_0|^2 \gg 1$ (with $k = 2\pi n/\lambda$ referring to light inside the ferromagnet). In the present example, $|kw_0| \simeq 2$ is near the limit of validity of the local gradient approximation, but the values of w_0 expected in iron alloys are substantially higher [9].

Figure 4 shows the dependence of $E_y^1(0)$, calculated at the image center, on the wall half-width w_0. The solid line shows the ratio $|E_y^1(0)/E_y^{1a}(0)|$, quite close to 1 in the range of w_0 corresponding to domain walls in iron alloys in the original experiment [1]. On the other hand, in very narrow walls, the ratio $|E_y^1(0)/E_y^{1a}(0)|$ decreases with decreasing w_0 (i.e., due to diffraction broadening of the image, the magnitude of the central field $|E_y^1(0)|$ does not grow as fast as the magnetization gradient).

The phase of the image field ratio $E_y^1(0)/iQE_y^0$ (dashed line in Fig. 4) in wide walls remains the same as in the gradient approximation, but in very narrow walls it drops with decreasing w_0, indicating that $E_y^1(0)$ may be nearly in phase with $P_z^\infty = iQ\varepsilon_0 E_y^0$, the surface polarization charge density far from the wall (see Ref. [5] and Appendix A).

Theoretically, images of very narrow walls would be generated by the polarization very close to the surface [5], as $\phi(z)$ in Eqs. (6) and (7) would fall off as e^{-qz} for the prevalent very high q, $|q/k|^2 \gg 1$ in the $m_r'(q)$ spectrum. Such boundaries of width on only an interatomic scale are typical for ferroelectric domains [17], but not for ferromagnets, where domain walls are broadened by the exchange stiffness [7] and subsurface effects are important [1,11] in the whole light penetration depth.

Gradient approximations to the remaining terms in Eqs. (6) and (7) are analogous to Eq. (8). Equation (6b) corresponds to domain boundaries with variable component m_y (normal to the wall line). The result obtained by supplementing $m_x E_y^0$ with $-m_y E_x^0$ is

$$E_y^{1(mx,y)}(y) = B\left(\frac{\partial m_y}{\partial y}E_x^0 - \frac{\partial m_x}{\partial y}E_y^0\right). \tag{9}$$

The same approximation in the polar Eqs. (7a) and (7b), $k' \simeq k$ and $t_{x,y} \simeq n/(n+1) = t_0$, gives analogous equations for the local $E_r^1(y)$ and $m_z(y,z)$ from Eq. (5). Then integration per parts over z gives [15] two terms in each equation,

$$E_y^{1(mz)} = \frac{1}{2}\left(-iQt_0 m_z + B\frac{\partial m_z}{\partial z}\right)E_x^0 \tag{10a}$$

$$E_x^{1(mz)} = \frac{1}{2}\left(iQt_0 m_z - B\frac{\partial m_z}{\partial z}\right)E_y^0. \tag{10b}$$

The first terms involve the surface magnetization and prevail in the bulk Kerr effect (e.g., discussed in Ref. [5]). The second terms describe the effect of a subsurface polar gradient and have a decisive role in the symmetry of the V-line images.

B. Symmetry of wall images

If $\mathbf{E}^0$ is applied along the polarizer axis ξ (Fig. 2), the bracket in Eq. (9) equals $-(\partial m_\eta/\partial y)E_\xi^0$. Since the vector $\mathbf{E}^1$ points along the gradient axis y, its component E_η^1 is proportional to the corresponding component of the gradient (i.e., to

the slope along the analyzer axis η). The observed contrast generated by purely in-plane gradient is thus determined as

$$E_\eta^{1(mx,y)} = -B\frac{\partial m_\eta}{\partial \eta}E_\xi^0, \tag{11}$$

which reproduces qualitatively only the last term in the empirical Eq. (2). This is because the in-plane gradient model assumed in Eq. (9) is not sufficient in cases involving head-on magnetization structure at the surface, as shown schematically in Fig. 1 (i.e., longitudinal gradient components $\partial m_y/\partial y$). Such **m** structure also contains polar magnetization in order to eliminate the divergence of **m** and the associated stray-field energy. The conditions postulated in the original micromagnetic theory [7] are

$$\mathrm{div}\mathbf{m} = 0 \tag{12a}$$

$$m_z(z=0) = 0, \tag{12b}$$

respectively, for the magnetic volume and for its planar surface at $z = 0$. The first condition requires that nonvanishing $\partial m_y/\partial y$ be compensated by opposite values of polar $\partial m_z/\partial z$. The second condition implies that the subsurface polar Kerr effect is determined by the polar gradient terms alone in Eqs. (10a) and (10b). The contrast generated by the polar gradient supplementing Eq. (11) is

$$E_\eta^{1(mz)} = -\frac{1}{2}B\frac{\partial m_z}{\partial z}E_\xi^0. \tag{13}$$

In the flux-closure structures the polar and planar gradients are correlated,

$$-\frac{\partial m_z}{\partial z} = \frac{\partial m_\xi}{\partial \xi} + \frac{\partial m_\eta}{\partial \eta}\left(=\frac{\partial m_y}{\partial y}\right). \tag{14a}$$

Substitution to Eq. (13) and addition with Eq. (11) gives

$$E_\eta^{1(mx,y,z)c} = \frac{1}{2}B\left(\frac{\partial m_\xi}{\partial \xi} - \frac{\partial m_\eta}{\partial \eta}\right)E_\xi^0 \tag{14b}$$

in agreement with both terms in the empirical Eq. (2). The superscript c indicates that m_z and m_y are correlated according to the conditions in Eq. (12).

Explicit angular dependence of the integrated MO amplitudes corresponding to Eq. (4c) follows from Eq. (14b) like in Sec. II, with two refinements. It has slightly wider validity than the local gradient approximation [16], and it may be written separately for the planar and polar gradient contributions.

The contrast caused by gradient of m_x (parallel to wall) is obtained from Eqs. (6a) or (8), with the detected $E_\eta^1 = E_y^1\sin\gamma$ and the primary field component E_y^0 derived from the applied field (parallel to the polarizer axis) (Fig. 2) as $E_y^0 = E_\xi^0\cos\gamma$. Consequently,

$$\int E_\eta^{1(mx)}dy = \frac{1}{2}BS_xE_\xi^0\sin 2\gamma \tag{15}$$

in accordance with the first term in Eq. (4c).

Analogously, for the contrast caused by variable component m_y (normal to the wall line), Eq. (6b) or the first term in Eq. (9), with the active E_x^0 equal to $-E_\xi^0\sin\gamma$, imply

$$\int E_\eta^{1(mx)}dy = BS_yE_\xi^0\sin^2\gamma, \tag{16}$$

which does not reproduce the last term in Eq. (4c). Diffraction on variable m_y component alone would produce only black lines (or only white lines, depending on the sign of S_y), with maxima at $\gamma = \pm 90^\circ$, while the experimental results [1] showed alternating black and white lines at $\gamma = \pm 90^\circ$ and at 0 and 180°.

In the flux-closure structures satisfying the conditions in Eqs. (12) and (14a), substitution of the last term in Eq. (14a) to Eq. (13) and integration across the image width gives a constant polar contribution

$$\int E_\eta^{1(mz)c}dy = -\frac{1}{2}BS_yE_\xi^0. \tag{17}$$

Addition of this constant term modifies the angular dependence in Eq. (16) to

$$\int E_\eta^{1(my,z)c}dy = -\frac{1}{2}BS_yE_\xi^0\cos 2\gamma, \tag{18}$$

in accord with the last term in Eq. (4c) and with a theoretical estimate of the empirical parameter P in Eqs. (4c) and (2), here equal to $\varepsilon B/2$ and B defined in Eq. (8b).

IV. CONCLUSION

The interpretation [1] of the unexpected domain wall images proposed additional MO terms $D^{(s)}$ in the dielectric law, Eq. (2), caused by microscopic MO currents. The present argument supports the derivation [6,10] of such terms from macroscopic currents, as $D^s = \varepsilon E^1$ where E^1 follows from Maxwell's equations and the classical MO dielectric law, Eq. (1), under two simplifying conditions reflecting two rules postulated in micromagnetics [7]: weakness of the magnetization gradient (due to ferromagnetic exchange stiffness) and magnetic flux closure (eliminating magnetostatic stray-field energy). The weak gradient condition is not applicable to hypothetical infinitely thin walls [5] and to ferroelectric domain boundaries [17] of atomic dimensions.

The correlation of planar and polar **m** gradient implied by the flux closure rules is essential for the anomalous symmetry of the V-line images and for the proportionality of their intensity to the difference of **m** components parallel to the planar gradient, called S_y in Eqs. (4c) and (18). Images of such planar gradient alone, without the flux-closing participation of polar m_z, were predicted [10] to have lower symmetry, as in Eq. (16), but they were not observed in spontaneous domain structures. Such low-symmetry contrast was only recently reported [18] in thin NiFe films in which stripes of opposite **m** directions perpendicular to the stripe axis were artificially stabilized by exchange bias [18–20] (from an antiferromagnetic overlayer structured by local ion irradiation in magnetic field).

Also the structure of Bloch walls with no net change of m_y normal to the wall is affected by the flux closing tendency [21–25]. The simple analytic model used in the illustration in Sec. III A does not describe the structure correctly in the surface region. Besides the gradient of m_x shown in Fig. 3 the classical model [7] involves polar m_z equal to $\pm 1/\cosh(y/w_0)$. If this were valid for all $z > 0$, the bulk polar Kerr effect caused by the wall core would have integrated amplitude exceeding the gradient effect (in relatively wide walls), but

the condition (12b) would be violated. The polar Kerr contrast is not observed [1], because directly at the surface the **m** direction in the wall rotates in the x-y plane like in Néel walls in thin films, and in the subsurface region the m_z and m_y components are again correlated so as to avoid divergence of **m**. The surface Néel caps of Bloch walls in iron and its alloys have vortex features theoretically predicted [21,22], confirmed by micromagnetic simulation [23–25] as well as by scanning electron microscopy with polarization analysis [23,24] and recently also discussed in the context of nanostructured iron particles [26]. Numerical simulation of MO images of complex micromagnetic structures have been reported for thin film vortex walls [27] and for a V-line model in iron [28].

APPENDIX

The amplitudes from Eq. (5) are sought in the form

$$E_x^1(q,z) = e_x^+(z)e^{ik'z} + e_x^-(z)e^{-ik'z}. \tag{A1a}$$

Such amplitudes with constant $e_r^\pm, h_r^\pm$ are solutions without the MO term in Maxwell's equation $\mathrm{rot}\mathbf{H}^1 + \mathrm{i}\omega\varepsilon\mathbf{E}^1 = \mathrm{I}\omega\mathbf{P}^m$. The MO right-hand side implies inclusion of additional derivatives on the left-hand side, like

$$\frac{de_x^+}{dz}e^{ik'z} + \frac{de_x^-}{dz}e^{-ik'z} = D(e_x). \tag{A1b}$$

Maxwell's equations lead to the set of two pairs,

$$D(h_y) = i\omega P_x^{(m)}(q,z) \tag{A2a}$$

$$D(e_x) = 0 \tag{A2b}$$

$$D(h_x) = -i\omega P_y^{(m)}(q,z) \tag{A3a}$$

$$D(e_y) = -iq P_z^{(m)}(q,z)/\varepsilon \tag{A3b}$$

where $D()$ is the symbol defined in (A1b) and the amplitudes satisfy additional paired relations, $h_x^\pm = \mp Y e_y^\pm/\gamma'$ and $h_y^\pm = \pm\gamma' Y e_x^\pm$, with $Y = \omega\varepsilon/k$ and $\gamma' = k'/k$, allowing elimination of $h_r^\pm$. The final equations (6, 7). follow as

$$E'^1_{x,y}(q,0) = -T_{x.y}\int_0^\infty \frac{de^-_{x,y}}{dz}dz \tag{A4}$$

with $T_{x.y}$ derived from Fresnel's transmission coefficients and with explicit $\mathbf{P}'^{(m)}(q,z) = iQ\varepsilon[\mathbf{m}'(q,z)\times\mathbf{E}^0]e^{ikz}$. The resulting coefficients in Eqs. (6) and (7) are: $t_y = n/(n+\gamma/\gamma_0)$ and $t_x = n/(n\gamma+\gamma_0)$ with $\gamma_0 = [1-(q\lambda/2\pi)^2]^{1/2}$.

Equations like (A2) and (A3) were discussed earlier [11,14]. While Eqs. (A2a) and (A3a) result from the $x-$,$y-$components of $\mathrm{rot}\mathbf{H}^1 + \mathrm{i}\omega\varepsilon\mathbf{E}^1 = \mathrm{I}\omega\mathbf{P}^m$, its $z-$component

$$\frac{\partial H_x^1}{\partial y} - i\omega\varepsilon E_z^1 = i\omega P_z^{(m)} \tag{A5}$$

shows that E_z^1 has two parts: the diffracted field of the form (A1a), proportional to $\partial H_x^1/\partial y$, and the depolarizing $E_z^{(V)} = -P_z^{(m)}/\varepsilon$. Equations (A2b) and (A3b) result from $\mathrm{rot}\mathbf{E}^1 - \mathrm{i}\omega\mu\mathbf{H}^1 = 0$ with E_z^1 substituted from (A5). The field $E_z^{(V)}$ contributes to the Voigt effect and reduces P_z: far from the domain wall, $P_z^\infty = P_z^{(m)}\varepsilon_0/\varepsilon$ is n^2 times less than $P_z^{(m)}$.

[1] R. Schäfer and A. Hubert, Phys. Status Solidi A **118**, 271 (1990); R. Schäfer, M. Rührig, and A. Hubert, IEEE Trans. Magn. **26**, 1355 (1990).

[2] A. Thiaville, A. Hubert, and R. Schäfer, J. Appl. Phys. **69**, 4551 (1991).

[3] V. Kamberský, Phys. Status Solidi A **123**, K71 (1991).

[4] Q. M. Zhong, A. S. Arrott, B. Heinrich, and Z. Celinski, J. Magn. Magn. Mater. **104–107**, 1837 (1992).

[5] I. Banno, Phys. Rev. A **77**, 033818 (2008); **77**, 033818 (2011).

[6] V. Kamberský, Phys. Status Solidi A **125**, K117 (1991); J. Magn. Magn. Mater. **104–107**, 311 (1992); **125**, 239 (1993).

[7] L. D. Landau and E. Lifshitz, Phys. Z. Sovietunion **8**, 153 (1935).

[8] W. F. Brown, *Micromagnetics* (Wiley, New York,1963).

[9] A. Hubert and R. Schäfer,*Magnetic Domains* (Springer, Berlin, 1998).

[10] L. Wenzel, V. Kamberský, and A. Hubert, Phys. Status Solidi A **151**, 449 (1995); V. Kamberský, L. Wenzel, and A. Hubert, J. Magn. Magn. Mater. **189**, 149 (1998).

[11] G. Träger, L. Wenzel, and A. Hubert, Phys. Status Solidi A **131**, 201 (1992); A. Hubert and G. Träger, J. Magn. Magn. Mater. **124**, 185 (1993).

[12] cf. last item in Ref. [6].

[13] A. Thiaville, F. Boileau, J. Miltat, and L. Arnaud, J. Appl. Phys. **63**, 3153 (1988).

[14] J. F. Cochran and J. R. Dutcher, J. Magn. Magn. Mater. **73**, 299 (1988).

[15] This argument was suggested by A. Thiaville in private correspondence concerning Ref. [6].

[16] Integration of $\partial m_{x,y}/\partial y$ over y giving $-S_{x,y}$ may be done before integration over z in Eqs. (6) and (7), in which $S_{x,y}$ are constant (even if the gradient components vary).

[17] I. Banno and K. Fujima, Phys. Rev. A **78**, 033816 (2008).

[18] R. Schäfer, C. Hamann, J. McCord, L. Schultz, and V. Kamberský, New J. Phys. **12**, 053006 (2010).

[19] A. Ehresmann, I. Krug, A. Kronenberger, A. Ehler, and D. Engel, J. Magn. Magn. Mater. **280**, 369 (2004).

[20] J. McCord, R. Schäfer, K. Theiss-Bröhl, H. Zabel, J. Schmalhorst, V. Höink, H. Brückl, T. Weis, D. Engel, and A. Ehresmann, J. Appl. Phys. **97**, 10K102 (2005).

[21] A. E. LaBonte, J. Appl. Phys. **40**, 2450 (1969).

[22] A. Hubert, Phys. Stat. Sol. **32**, 519 (1969); **38**, 699 (1970).

[23] M. R. Scheinfein, J. Unguris, K. J. Coakley, and D. T. Pierce, Phys. Rev. Lett. **63**, 668 (1989).

[24] M. R. Scheinfein, J. Unguris, J. L. Blue, K. J. Coakley, D. T. Pierce, R. J. Celotta, and P. J. Ryan, Phys. Rev. B **43**, 3395 (1991).

[25] W. Rave and A. Hubert, J. Magn. Magn. Mater. **184**, 179 (1998).

[26] A. S. Arrott, J. Appl. Phys. **109**, 07E135 (2011).

[27] cf. first item in Ref. [10].

[28] L. Wenzel, J. McCord, K. Ramstöck, and A. Hubert, IEEE Trans. Magn. **33**, 3274 (1997).